The fluorescence ubiquitination-based cell cycle indicator (Fucci) is a fluorescent probe that detects the various stages of the cell cycle in living cells (14). In this system, geminin, a nuclear protein enriched in the $S/G_2/M$ phases, and Cdt1, which is enriched in the G_0/G_1 phase, are marked by green and red fluorescent proteins, respectively.

In this study, we exploited these advanced imaging technologies to analyze the therapeutic mechanism of IFN-α against IFN-α-susceptible HCCs, particularly in association with the cell cycle.

EXPERIMENTAL PROCEDURES

Cell Lines and Reagents—The human HCC cell line HuH7 was obtained from the Japan Cancer Research Resources Bank (Tokyo, Japan). These cells were maintained in Dulbecco's modified Eagle's medium supplemented with 10% fetal bovine serum, 100 units/ml penicillin, and 100 mg/ml streptomycin at 37 °C in a humidified incubator with 5% CO_2 in air. Cells were treated with either purified human IFN-α (kindly provided by Otsuka Pharmaceutical Co., Tokyo, Japan) at final concentrations of 10–10,000 IU/ml or 5-FU (Wako Pure Chemical Industries, Osaka, Japan) at final concentrations of 10, 100, or 1000 μM. To synchronize the cell cycle of HuH7 cells, the cells were treated with aphidicolin (Calbiochem) at a final concentration of 1.6 μg/ml for 24 h.

TABLE 1
List of primer sequences used for RT-PCR analysis in this study

Primer	Sequence
GAPDH forward primer	5′-GTCGGAGTCAACGGATTTGGT-3′
GAPDH reverse primer	5′-GCCATGGGTGGAATCATATTGG-3′
IFNAR1 forward primer	5′-ATTTACACCATTTCGCAAAGCTC-3′
IFNAR1 reverse primer	5′-TCCAAAGCCCACATAACACTATC-3′
IFNAR2 forward primer	5′-GAAGGTGGTTAAGAACTGTGC-3′
IFNAR2 reverse primer	5′-CCCGCTGAATCCTTCTAGGACGG-3′
TAp63 forward primer	5′-GTCCCAGAGCACACAGACAA-3′
TAp63 reverse primer	5′-GAGGAGCCGTTCTGAATCTG-3′
ΔNp63 forward primer	5′-CTGGAAAACAATGCCCAGAC-3′
ΔNp63 reverse primer	5′-GGGTGATGGAGAGAGAGCAT-3′
p21 forward primer	5′-GACACCACTGGAGGGTGACT-3′
p21 reverse primer	5′-CAGGTCCACATGGTCTTCCT-3′
PUMA forward primer	5′-GCCAGATTTGTGAGACAAGAGG-3′
PUMA reverse primer	5′-CAGGCACCTAATTGGGCTC-3′

Generation of IFNAR2-expressing Fucci-introduced Cell Lines—Full-length cDNA of the human interferon-α/β receptor β-chain precursor (IFNAR2), obtained from Kazusa DNA Research Institute (Chiba, Japan), was inserted in front of the intraribosomal entry site (IRES) of the retroviral vector, pMX-IRES-Puro, using EcoRI sites to obtain pMX-IFNAR2. Replication-defective retroviruses were generated by transient transfection of pMX-IFNAR2 or pMX-IRES-Puro (control) into PLAT-A cells using FuGene 6 reagent (Promega, Tokyo, Japan) (15). HuH7 cells were transduced with the resulting retroviruses as described previously (16) and positively selected and expanded in the presence of 2 μg/ml puromycin. mAG-hGeminin mKO2-hCdt1 (kindly provided by Dr. Miyawaki, RIKEN-BSI, Japan) was cloned into the lentiviral vector CSII-EF-MCS (kindly provided by Dr. Miyoshi, RIKEN-BRC, Japan) and transfected into HEK293T cells with packaging plasmids (17). Lentiviral supernatant was used to transduce HuH7 cells. To select double-transduced cells, double-positive (Fucci green (mAG) and Fucci red (mKO2)) HuH7 cells were subsequently purified using a FACSAria cell sorter (BD Biosciences), as described below.

Quantitative Real-time RT-PCR and Immunoblot Analyses—Quantitative real-time RT-PCR (qRT-PCR), preparation of cell lysates, and immunoblot analyses were performed according to a previous report (18). All oligonucleotides used for qRT-PCR analyses were designed to amplify cDNA across exon-intron junctions, as described in Table 1. All data were normalized against internal GAPDH controls. Relative expression levels of IFNAR1 and IFNAR2 of WT controls were set as 1, and mRNA levels of mock and IFNAR2-expressing HuH7 samples were accordingly plotted as a -fold change. A full-length human p63 cDNA sequence, obtained from the Kazusa DNA Research Institute (Chiba, Japan), was transfected into HuH7 cells using FuGENE6 (Promega, Tokyo, Japan), according to the manufacturer's protocol. Cell lysates ware collected 1 day after transfection to perform qRT-PCR analyses.

To analyze activation of STAT1, -2, and -3, we performed immunoblot analyses using the primary antibodies described in Table 2. Mock control and IFNAR2-expressing cells were cultured in medium containing 10% FBS for 2 days and then in

TABLE 2
List of antibodies used for immunoblotting analysis in this study

Antibody	Source
Mouse anti-human IFNAR1 (H-11)	Santa Cruz Biotechnology
Rabbit anti-human IFNAR2	Otsuka Pharmaceutical
Rabbit anti-human STAT1 (CST 9172)	Cell Signaling Technology
Rabbit anti-human phospho-STAT1 (CST 9171)	Cell Signaling Technology
Rabbit anti-human STAT2 (CST 4441)	Cell Signaling Technology
Rabbit anti-human phospho-STAT2 (CST 4549)	Cell Signaling Technology
Rabbit anti-human STAT3 (CST 4904)	Cell Signaling Technology
Rabbit anti-human phospho-STAT3 (CST 9145)	Cell Signaling Technology
Mouse IgG-HRP conjugated anti-human actin	GenScript USA Inc.
Mouse anti-human p53 (DO-1)	Santa Cruz Biotechnology
Mouse anti-human p63 (4A4)	Santa Cruz Biotechnology
Mouse anti-human p21 (187)	Santa Cruz Biotechnology
Rabbit anti-human caspase-3 (CST 9662)	Cell Signaling Technology
Rabbit anti-human active caspase-3 (CST 9661)	Cell Signaling Technology
Rabbit anti-human caspase-7 antibody (CST 9492)	Cell Signaling Technology
Rabbit anti-human active caspase-7 antibody (CST 9492)	Cell Signaling Technology
Rabbit anti-human p38 (Poly 6224)	BioLegend
Rabbit anti-human phospho-p38 (CST 4631)	Cell Signaling Technology
HRP-labeled polyclonal secondary anti-rabbit (NA934V)	GE Healthcare
HRP-labeled anti-mouse-specific antibodies (NA931V)	GE Healthcare

FBS-free medium for 2 h. They were then incubated in medium with IFN-α (100 IU/ml) for 0–80 min, and the cells were lysed with mammalian lysis buffer (Promega, Tokyo, Japan). Cell lysates (10 μg of protein/lane) were loaded on 4–20% Mini-PROTEAN® TGX™ gels (Bio-Rad), separated by electrophoresis, and blotted onto a nitrocellulose membrane. The membrane was blocked in PVDF Blocking Reagent for Can Get Signal® (Toyobo, Osaka, Japan) for 1 h at room temperature and incubated with the specific antibodies in Can Get Signal® Immunoreaction Enhancer Solution 1™ (Toyobo, Osaka, Japan) overnight at 4 °C. After washing in 1× TBS-T, the membranes were incubated with HRP-labeled polyclonal secondary anti-rabbit (NA934V; GE Healthcare) or anti-mouse-specific antibodies (NA931V; GE Healthcare). Chemiluminescence was detected with an ECL Prime Kit (PerkinElmer Life Sciences) using an LAS4000 imaging system (GE Healthcare).

To analyze IFN-α/IFNAR2 signaling in G_0/G_1 or $S/G_2/M$ phases, IFNAR2-expressing Fucci-labeled HuH7 cells were treated with or without IFN-α (1,000 IU/ml) and sorted by FACS 24 h after treatment. Immunoblotting was performed as described above. The primary antibodies are listed in Table 2.

To deplete p63 expression, we performed RNAi with MISSION siRNA (Hs_TP63_6771 for TP63-specific and MISSION siRNA Universal Negative Control 1 for control; Sigma). RNA duplexes were transfected into IFNAR2-expressing HuH7 cells with RNAi MAX (Invitrogen) according to the manufacturer's instructions. After 24 h of transfection, cells were treated with 1,000 IU/ml IFN for 0, 24, or 48 h. qRT-PCR and immunoblot analyses were performed as described above (18).

Time Lapse Imaging—Cells ($1.5 \times 10^4/cm^2$) were grown overnight at 37 °C before imaging on a glass bottom dish in phenol red-free Dulbecco's modified Eagle's medium containing 10% FBS. Time lapse imaging was performed every 30 or 60 min with a confocal A1 microscope system (Nikon, Tokyo, Japan) equipped with a humidified imaging chamber (Nikon) at 37 °C, 5% CO_2 in air. Time lapse images were analyzed using Nikon NIS-Elements software (Nikon).

Cells were defined as apoptotic if they showed morphological changes, such as cell shrinkage and fragmentation into membrane-bound apoptotic bodies. The fluorescent signal detected in apoptotic cells was used to identify the cell cycle phases at which apoptosis occurred (*red*, G_0/G_1; *green*, $S/G_2/M$). To analyze the relationship between the cell cycle and apoptosis, each individual cell was tracked, and cell cycle changes and cell fate were monitored for 72 h. The frequency of cell death was calculated by dividing the initial total cell number in the visual field at $t = 0$ by the number of apoptotic cells for each cell cycle phase at the time of cell death ($t = 0$ until $t = 72$ h).

Flow Cytometry—To analyze the DNA content of Fucci-transfected HuH7 cells, we stained the cells with Hoechst 33342 (final concentration, 3.6 μg/ml; Invitrogen). After incubation for 30 min, cells were harvested and analyzed using a FACSCanto II flow cytometer (BD Biosciences). Both mKO2 and mAG were excited by a 488-nm laser, and Hoechst 33342 dye was excited by a 325-nm laser. Fluorescence signals were collected at 530 nm (530/28 BP) for mAG, at 575 nm (575/26 BP) for mKO2, and at 400 nm (380 LP) for Hoechst 33342 dye (14).

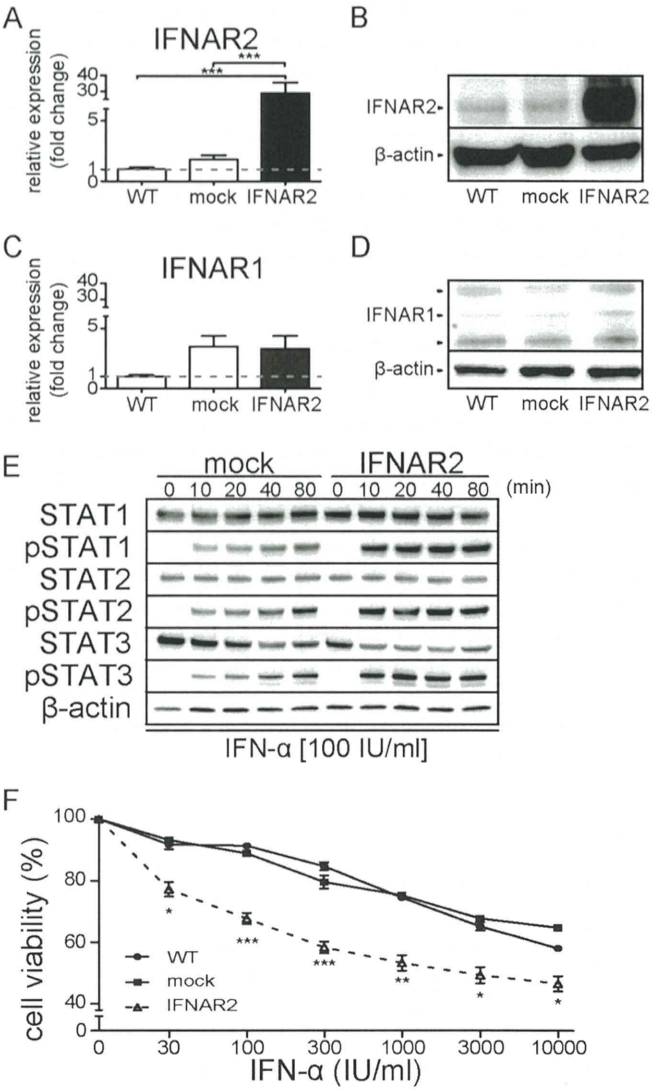

FIGURE 1. **Exogenous expression of IFNAR2 in HuH7 cells confers susceptibility to IFN-α treatment.** *A*, relative levels of IFNAR2 mRNA detected by qPCR in WT-, empty vector (mock)-, and IFNAR2-transfected HuH7 cells. Each *bar* represents the mean ± S.E. (*error bars*) of three individual experiments ($n = 3$ for each). ***, $p < 0.005$. *B*, Western blot detection of IFNAR2 protein from total cellular lysates of non-transfected (WT), empty vector transfected (mock), and IFNAR2-transfected HuH7 cells. *C*, relative amount of IFNAR1 mRNA detected by qPCR in WT and expressing empty vector (mock) or IFNAR2 HuH7 cells. Each bar represents the mean ± S.E. (*error bars*) of three individual experiments ($n = 3$ for each). *D*, Western blot detection of IFNAR1 protein from total cellular lysates of WT-, mock-, and IFNAR2-transfected HuH7 cells. *E*, Western blot detection of STAT1, -2, and -3 proteins and their phosphorylated forms from whole cell lysates of mock- or IFNAR2-transfected HuH7 cells. The lysates were collected at each time point after treatment with 100 IU/ml IFN-α. *F*, viability of HuH7 cells was examined by an MTT assay after treatment with different doses of IFN-α for 72 h. Cell viability is presented as the ratio of IFN-α-treated cells relative to untreated control cells. Statistical significance was determined between mock- and IFNAR2-expressing HuH7 cells at each IFN-α concentration, and the IC_{70} was determined for IFN-α-treated cells as follows: WT, 1,998.7 ± 200.5 IU/ml; mock, 2,389.1 ± 321.8 IU/ml; IFNAR2, 90.1 ± 36.1 IU/ml. Each *bar* represents the mean ± S.E. (*error bars*) of three individual experiments ($n = 3$ for each). *, $p < 0.05$; **, $p < 0.01$; ***, $p < 0.005$.

Preparative FACS sorting was performed using a FACSAria (BD Biosciences) cell sorter equipped with a 488-nm laser using 530/30BP or 585/42BP filters, respectively. The data were analyzed using FlowJo software (Tree Star, Inc., Ashland, OR).

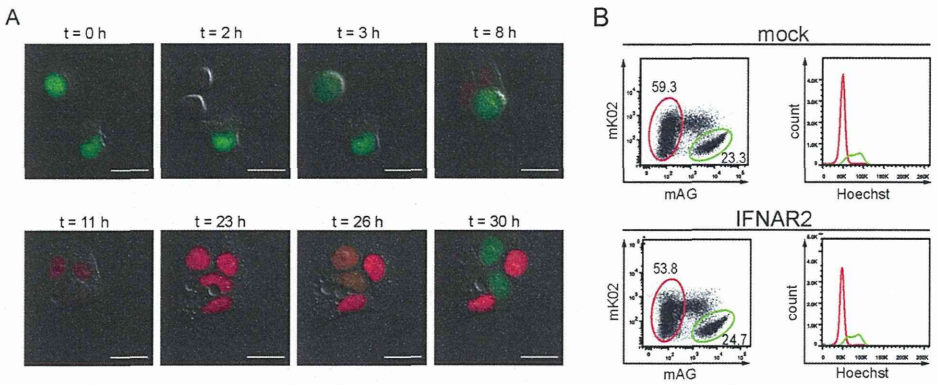

FIGURE 2. **Visualization of the cell cycle using the Fucci system.** *A*, representative images of cell cycle changes in IFNAR2-expressing Fucci-introduced HuH7 cells visualized by confocal time lapse imaging. *Red fluorescence* (mKO2-hCdt1) and *green fluorescence* (mAG-hGem) indicate G_0/G_1 and $S/G_2/M$ phases of the cell cycle, respectively. *B*, FACS analyses of mock- or IFNAR2-expressing Fucci-introduced HuH7 cells, identifying at least two distinct populations: mKO2-positive and mAG-negative (*red circled*) *versus* mKO2-negative and mAG-positive (*green circled*). The DNA content of each population was analyzed by staining with Hoechst 33342 dye (histograms). The *red* and *green lines* (in the *right panels*) represent histograms of the cells *circled* in *red* and *green* (in the *left panels*). These data confirmed that *red circled* cells (*i.e.* mKO2-positive G_1/G_0 cells) and *green circled* cells (*i.e.* mAG-positive $S/G_2/M$ cells) have 2N-DNA and 4N-DNA contents, respectively. *Numbers* indicate the frequencies (%) of living cells.

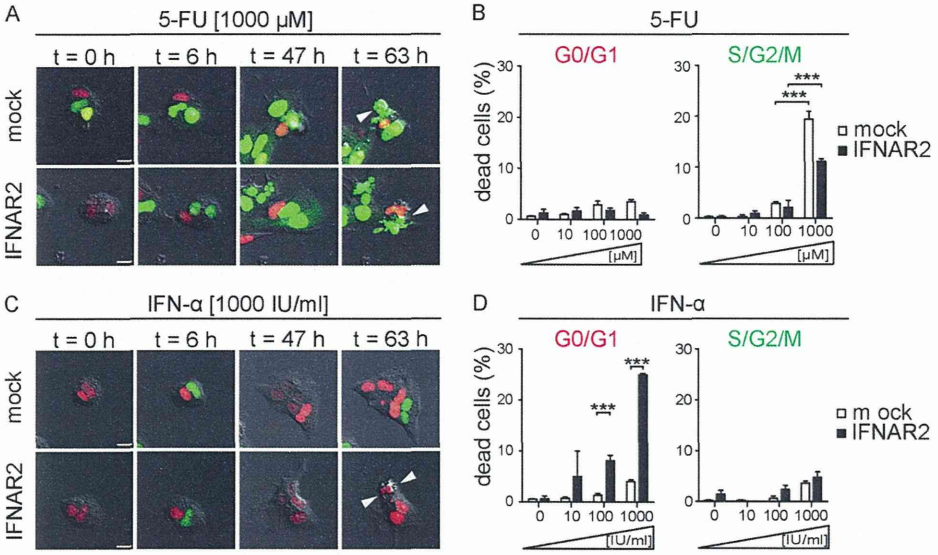

FIGURE 3. **Confocal time lapse imaging of apoptosis induction by 5-FU or IFN-α in IFNAR2-expressing Fucci-introduced HuH7 cells.** *A*, representative images from confocal time lapse imaging of Fucci-introduced IFNAR2-expressing HuH7 cells treated with 5-FU (1,000 μM) for 72 h. Red fluorescence (mKO2-hCdt1) and green fluorescence (mAG-hGeminin) represent the G_0/G_1 phases and $S/G_2/M$ phases of the cell cycle, respectively. *Arrowheads*, apoptotic cells. *Scale bar*, 10 μm. *B*, quantification of 5-FU-induced apoptosis at various phases of the cell cycle monitored by confocal time lapse imaging. Each *bar* represents the mean ± S.E. (*error bars*) of three individual experiments ($n = 3$). *C*, representative confocal time lapse images of Fucci-introduced IFNAR2-expressing HuH7 cells treated with IFN-α (1,000 IU/ml) for 72 h. *Arrowheads* indicate apoptotic cells. *Scale bar*, 10 μm. *D*, quantification of IFN-α-induced apoptosis at various phases of the cell cycle monitored by confocal time lapse imaging. Each *bar* represents the mean ± S.E. (*error bars*) of three individual experiments ($n = 3$).

3-(4,5-Dimethylthiazol-2-yl)-2,5-diphenyltetrazolium Bromide (MTT) Assay—The MTT assay was performed with the Cell Proliferation Kit 1 (Roche Applied Science) according to the manufacturer's protocol. In short, cells (1×10^3 cells/96-well dish) were grown overnight at 37 °C in a 96-well dish. Following treatment with or without IFN-α (30, 100, 300, 1,000, 3,000, and 10,000 IU/ml) for 72 h at 37 °C, cells were labeled with MTT-labeling reagent (MTT final concentration, 0.5 mg/ml; Roche Applied Science) for 4 h at 37 °C and subsequently solubilized with Solubilization Solution (Roche Applied Science) for 16 h at 37 °C. The absorbance was measured in a microplate reader (PowerScanHT; DS Pharma Biomedical, Osaka, Japan) at a wavelength of 550 nm with a 650-nm reference. The assays were carried out in 12 replicates at each IFN-α concentration in three individual experiments, and the results were plotted as a percentage of the absorbance relative to untreated controls. The concentration of IFN-α required to reduce the cell viability to 70% that of control cells (IC_{70}) was calculated from the spline curve generated using GraphPad Prism® software (GraphPad Software, Inc., La Jolla, CA).

Statistical Analyses—Differences between the control and treated groups were assessed by an unpaired Student's *t* test or Mann-Whitney *U* test and considered to be significant at $p < 0.05$ (*, $p < 0.05$; **, $p < 0.01$; ***, $p < 0.005$). Values are given as means ± S.E. Statistical analysis was performed using GraphPad Prism® software (version 5.0; GraphPad Software).

RESULTS

IFN-α Reduces the Viability of IFNAR2-expressing HCC Cells—To study the role of IFN-α in the induction of apoptosis of HCC cells, we transduced IFNAR2 into the human HCC cell

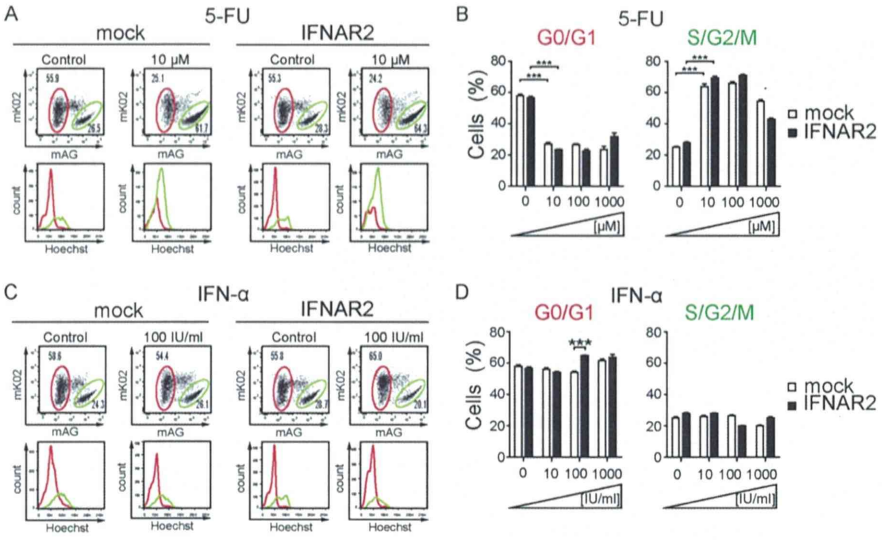

FIGURE 4. **Cell cycle analysis following 5-FU or IFN-α treatment using FACS.** *A* and *C*, representative dot plots from FACS analysis of mock- or IFNAR2-expressing Fucci-introduced HuH7 cells, 48 h after treatment with 10 μM 5-FU or 1,000 IU/ml IFN-α. The G_0/G_1 and $S/G_2/M$ populations were analyzed as described in the legend to Fig. 2. *B* and *D*, statistical analysis of four independent experiments 48 h after application of 5-FU (0, 10, 100, and 1,000 μM) or IFN-α (0, 10, 100, and 1,000 IU/ml). Bar graphs indicate the percentage of living cells in G_0/G_1 and $S/G_2/M$. Each *bar* represents the mean ± S.E. (*error bars*) of four independent experiments ($n = 4$). ***, $p < 0.005$.

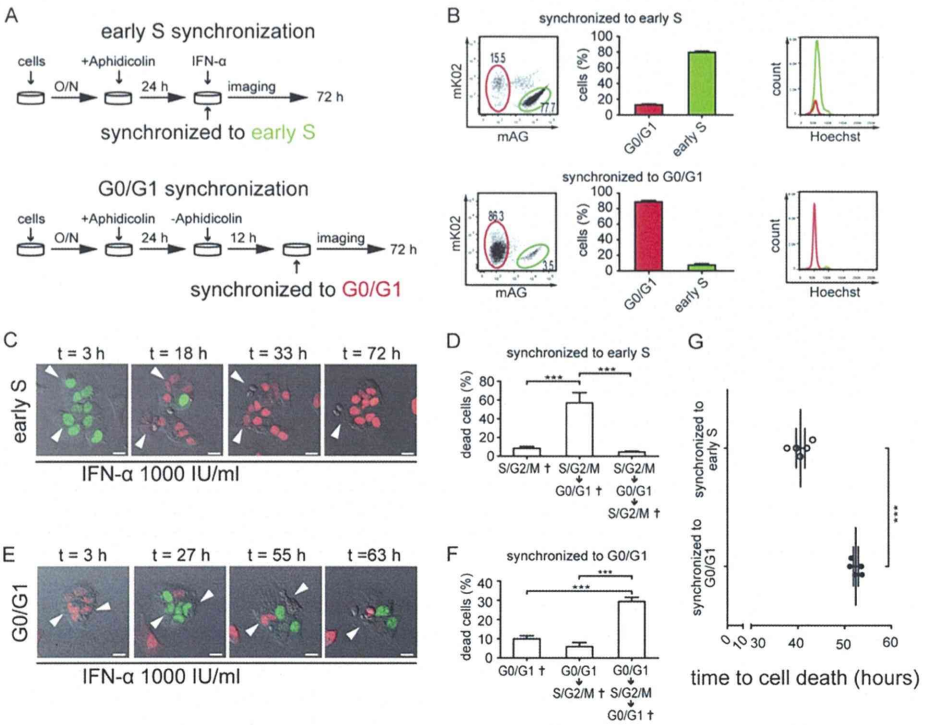

FIGURE 5. **Cell cycle synchronization revealed that IFN-α/IFNAR2 signaling acts on $S/G_2/M$ but induces apoptosis at the G_0/G_1 phases in HuH7 cells.** *A*, scheme of the protocol used to synchronize HuH7 cells to either early S phases (*top*) or to G_0/G_1 phases (*bottom*) by aphidicolin (1.6 μg/ml). *B*, confirmation of cell cycle synchronization upon aphidicolin treatment. IFNAR2-expressing Fucci-introduced HuH7 cells were analyzed by FACS. Cell cultures treated with aphidicolin for 24 h showed enrichment in the Fucci green population, whereas they were rather enriched in Fucci red when cultured for an additional 12 h in cells without aphidicolin. Bar graphs show the average values from five independent experiments. Cells were also analyzed by staining with Hoechst 33342 dye, representing the expected DNA content in each population. *C*, representative time lapse tracking images of early S-synchronized IFNAR2-expressing HuH7 cells treated with IFN-α (1,000 IU/ml) for 72 h. *Arrowheads*, apoptotic cells. *Scale bar*, 10 μm. *D*, frequency of cell death according to cell cycle phase. Relative numbers of cells that died in the first $S/G_2/M$ (*left*) and in the following G_1 (*middle*) and $S/G_2/M$ (*right*) phases are shown in the *columns*. Each *bar* represents the mean ± S.E. (*error bars*) of five individual experiments ($n = 5$). ***, $p < 0.005$. *E*, representative time lapse tracking images of G_0/G_1-synchronized IFNAR2-expressing HuH7 cells treated with IFN-α (1,000 IU/ml) for 72 h. *Arrowheads*, apoptotic cells. *Scale bar*, 10 μm. *F*, frequency of cell death in each cell cycle status. Relative numbers of cells that died in the first G_0/G_1 (*left*) and in the following $S/G_2/M$ (*middle*) and G_1 (*right*) phases are shown in the *columns*. Each *bar* represents the mean ± S.E. (*error bars*) of five individual experiments ($n = 5$). ***, $p < 0.005$. *G*, the time points of cell death induced by IFN-α after synchronized to early S phase or G_0/G_1 phase. Each *dot* shows the average of time points of cell death that were observed in time lapse tracking images of early S-synchronized or G_0/G_1-synchronized IFNAR2-expressing HuH7 cells treated with IFNA-α (1,000 IU/ml). Each *bar* represents the mean ± S.E. (*error bars*) of five individual experiments ($n = 5$). ***, $p < 0.005$.

line HuH7 with a constitutive retroviral expression vector for IFNAR2 (pMXs-IFNAR2) because the endogenous expression level of IFNAR2 in HuH7 cells is quite low (19). To confirm expression in HuH7 cells, we performed qPCR and immunoblot analyses. We obtained a HuH7 cell line expressing a higher level of IFNAR2, 30-fold higher in mRNA (Fig. 1*A*) and 9-fold higher in protein (Fig. 1*B*) than the mock control. Expression of IFNAR1 was also moderately increased in both the mock control and IFNAR2-expressing HuH7 cells (Fig. 1, *C* and *D*), possibly due to intrinsic cell responses against viral infection (20). To determine activation of the JAK/STAT signaling pathway upon IFN-α treatment of these cells, we performed immunoblot analyses to detect phosphorylation of STATs (STAT1, -2, and -3) (Fig. 1*E*). All STATs were phosphorylated in both the mock control and IFNAR2-expressing HuH7 cells, although the phosphorylation level was increased in IFNAR2-expressing HuH7 cells, indicating the function of exogenously expressed IFNAR2.

To confirm the responsiveness of these HuH7 cells to IFN-α treatment, we performed MTT assays (Fig. 1*F*). As expected, upon treatment with increasing concentrations of IFN-α, the viability of IFNAR2-expressing cells was significantly lower than that of WT and mock controls (Fig. 1*F*), indicating specific growth inhibition, such as apoptosis or cell cycle arrest induction through an IFN-α/IFNAR2 interaction. This result confirms that IFN-α negatively regulates cell viability in an IFNAR2-dependent manner and validates these IFNAR2-expressing HuH7 cells as a useful model with which to investigate the cellular responses of HCC to IFN-α therapy *in vitro*.

IFN-α Specifically Induces Apoptosis by an IFNAR2 Signaling Pathway at the G_0/G_1 Phases of the Cell Cycle—To examine the association between IFN-α action and cell cycle status, we introduced Fucci into the IFNAR2-expressing HuH7 cells and control (mock) HuH7 cells, both of which we have established (Fig. 1). Fucci-introduced IFNAR2-expressing HuH7 cells and mock controls allowed for tracking of individual cells over time and cell cycle changes during cell division by time lapse imaging using confocal microscopy (Fig. 2*A*). Furthermore, the DNA content (detected by a nuclear acid dye, Hoechst 33342) of Fucci-labeled HuH7 cells in the G_0/G_1 and $S/G_2/M$ phases varies according to the fluorescently indicated stages of the cell cycle in flow cytometric analyses (Fig. 2*B*), indicating the proper functioning of the Fucci system.

Concerning putative differential roles for IFN-α and 5-FU in effective clinical combination therapies for HCC, we performed *in vitro* time lapse imaging of Fucci-labeled IFNAR2-expressing HuH7 cells treated with IFN-α or 5-FU. Cells were defined as apoptotic if they showed morphological changes indicative of cell shrinkage and fragmentation into membrane-bound apoptotic bodies (21). First, we demonstrated that treatment with 5-FU, a nucleic acid analog that prevents cell division, led to accumulation of green ($S/G_2/M$) cells over time (Fig. 3*A* and supplemental Video 1) in a dose-dependent manner (Fig. 4, *A* and *B*). In addition, the cell death events (Fig. 3*A*, *arrowheads*) occurred preferentially in the green $S/G_2/M$ phases in both the control and IFNAR2-expressing HuH7 cells with comparable efficiency (Fig. 3*B*). These results are consistent with the conventional idea that nucleic acid analogs, such as 5-FU, block the

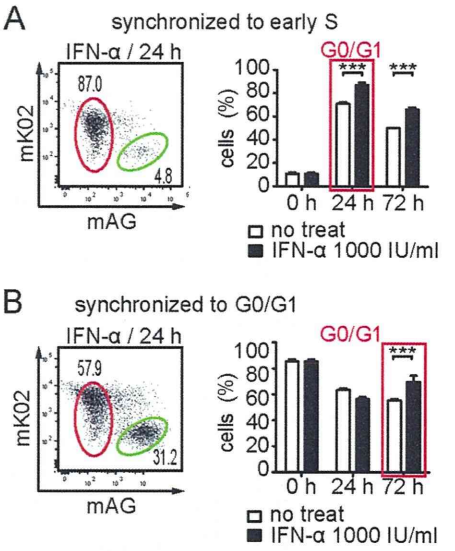

FIGURE 6. **FACS analysis after IFN-α treatment on cell cycle-synchronized cells.** *A*, time-dependent changes in cell cycle status of early S-synchronized cells. Cells were analyzed by FACS at the indicated time points with or without IFN-α treatment (1,000 IU/ml). Shown are a representative chart at 24 h (*left*) and the relative cell counts of the G_0/G_1 population (*right*). Each *bar* represents the mean ± S.E. (*error bars*) of three individual experiments ($n = 3$). ***, $p < 0.005$. *B*, time-dependent change in cell cycle status of G_0/G_1-synchronized cells with or without IFN-α treatment (1,000 IU/ml). A representative chart at 24 h (*left*) and the relative cell counts of the G_0/G_1 population (*right*). Each *bar* represents the mean ± S.E. (*error bars*) of three individual experiments ($n = 3$). ***, $p < 0.005$.

cell cycle at the S phase and exert cytotoxicity (22), and it was expected that this cytotoxic effect induced by 5-FU was not dependent on the expression of IFNAR2.

In contrast, IFN-α treatment resulted in an accumulation of red (G_0/G_1) IFNAR2-expressing HuH7 cells, and the results were not obvious in mock controls (Figs. 3*C* and 4 (*C* and *D*) and supplemental Video 2). Moreover, a high frequency of cell death in red (G_0/G_1) cells was also observed by time lapse imaging, albeit in only IFNAR2-expressing HuH7 cells (Fig. 3, *C* (*arrowheads*) and *D*). It should be noted that IFN-α treatment did not increase the rate of death of green ($S/G_2/M$) cells but resulted in an increased proportion of red (G_0/G_1) apoptotic cells at 100 or 1,000 IU/ml IFN-α, suggesting that IFN-α causes G_0/G_1 arrest.

These observations identified unique roles for IFN-α and 5-FU in inducing cell death at specific stages of the cell cycle. In addition, our data emphasize the importance of the IFN-α/IFNAR2 signaling pathway in regulating the efficiency of apoptosis induction at the G_0/G_1 phases of the cell cycle.

Cell Cycle Synchronization Revealed That IFN-α/IFNAR2 Signaling Acts on $S/G_2/M$ but Induces Apoptosis at the G_0/G_1 Phases in HuH7 Cells—To more precisely monitor the time course of the cell cycle-dependent IFN-α effect on IFNAR2-expressing HuH7 cells, we synchronized the cell cycle of HuH7 cells during G_0/G_1 to the early S boundary using aphidicolin, a reversible inhibitor of DNA polymerases (23). We were able to synchronize Fucci-transfected IFNAR2-expressing HuH7 cells to the early S phases (*green*) by the addition of aphidicolin for 24 h or to the G_0/G_1 phases (*red*) by removal of aphidicolin for 12 h (Fig. 5*A*). The relative populations of the cell cycle phases of the synchronized cells were evaluated by FACS, which indi-

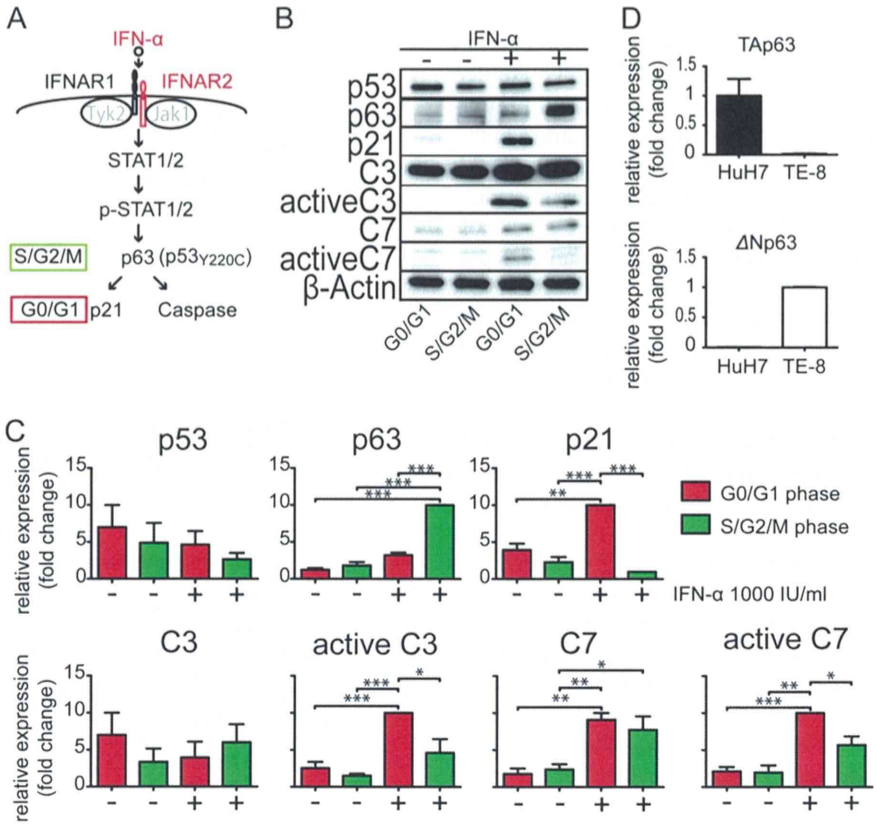

FIGURE 7. **Biochemical analyses of IFN-α/IFNAR2-induced signaling cascades in HuH7 cells.** *A*, schematic illustration of IFN-α-induced proapoptotic signaling, resulting in cell cycle arrest and apoptosis. *B*, expression of several critical signaling molecules activated by IFN-α, including p53, p63, p21, caspase-3 (*C3*), active caspase-3, caspase-7 (*C7*), active caspase-7, and β-actin (control). After culturing in the absence or presence of IFN-α (1000 IU/ml) for 24 h, IFNAR2-expressing Fucci-introduced HuH7 cells were sorted by FACS for the G_0/G_1 (mKO single positive) or $S/G_2/M$ (mAG single positive) and analyzed by Western blotting. *C*, densitometric analyses of Western blot data presented in Fig. 6*B*. The relative expression of each molecule was measured by ImageQuant TL version 7 (GE Healthcare). Each *bar* represents the mean ± S.E. (*error bars*) of three individual experiments ($n = 3$). *D*, relative mRNA expression levels of two isoforms of p63, TAp63 and ΔNp63, detected by qPCR in HuH7 and TE-8 cells. Each *bar* represents the mean ± S.E. (*error bars*) of three individual experiments ($n = 3$). *, $p < 0.05$; **, $p < 0.01$; ***, $p < 0.005$.

cated that 77.7 and 86.3% of cells were enriched to early S (*green*) or G_0/G_1 (*red*) by these methods, respectively (Fig. 5*B*).

Using this synchronization technique, we examined the effect of IFN-α exposure on the cell cycle of HuH7 cells. Most of the early S-synchronized cells (~57.1%) underwent apoptosis when they entered the next G_0/G_1 phase (Fig. 5, *C* (*arrowheads*) and *D*, and supplemental Video 3), suggesting that IFN-α-induced cell death occurs during mainly the G_0/G_1 phase. In contrast, a majority of the G_0/G_1-synchronized cells (~29.4%) died in the re-entered G_0/G_1 phase after going through the next $S/G_2/M$ phases (Fig. 5, *E* (*arrowheads*) and *F*, and supplemental Video 4). Concordantly, tracking of respective cell fates showed that cell deaths occurred faster in S phase-synchronized cells (40.6 ± 2.1 h) than in G_0/G_1-synchronized cells (52.4 ± 1.2 h) (Fig. 5*G*). We also checked the cell cycle status using FACS and found that IFN-α-induced accumulation of cells in the G_0/G_1 phase, which can be assumed to be a preapoptotic population, was detected earlier in the early S-synchronized cells (~24 h) (Fig. 6*A*), compared with the case with the G_0/G_1-synchronized cells (~72 h) (Fig. 6*B*). These results indicate that the $S/G_2/M$ phase is critical for receiving the "cell cycle arrest and death" signals from IFN-α, although the cells died mainly during the following G_0/G_1 phase.

Biochemical Analyses of IFN-α/IFNAR2- induced Signaling Cascades in HuH7 Cells—Finally, we assessed the molecular mechanisms underlying cell cycle-dependent IFN-α action. The interaction of IFN-α and IFNAR2 has been reported to activate the JAK/STAT signaling cascade, which is considered to be involved in G_1 arrest, leading to apoptosis (5) (Fig. 7*A*). To confirm the activation of this pathway, we performed immunoblotting for signaling components of the proapoptotic JAK/STAT pathways on IFNAR2-expressing Fucci-labeled HuH7 cells, which were used in the confocal time lapse imaging. Cells were treated or not treated with IFN-α for 24 h and separately collected for identification of G_0/G_1 or $S/G_2/M$ populations by cell sorting.

Expression of p53, which has been reported to play a central role in cell cycle arrest and apoptotic induction (6), was unaltered in HuH7 cells treated by IFN-α, irrespective of the cell cycle status (Fig. 7, *B* (*lane 1*) and *C*). This was probably because p53 in HuH7 cells carries a point mutation (Y220C) that renders it non-susceptible to IFN-α (24). Instead, we monitored the expression of p63, a molecule homologous to p53 (25, 26) and thus considered to play roles comparable with those of p53. We detected marked elevation of p63, especially during the $S/G_2/M$ phases (Fig. 7, *B* (*lane 2*) and *C*), suggesting that IFN-

α-induced apoptotic signals were activated preferentially in the S/G_2/M phase. In the case of p63, there are two distinct promoters that result in two different types of proteins with opposing functions (*i.e.* p53-like proteins containing the transactivation (TA) domain (TAp63) and inhibitory proteins lacking the TA domain) (ΔNp63) (27). In our HuH7 cells, only TAp63 was confirmed to be expressed both at the mRNA (Fig. 7*D*) and protein levels (data not shown). In contrast, the increase in p21, which has been shown to be responsible for G_1 arrest (28), and the activation of caspase-3 and -7 could be preferentially detected in the G_0/G_1 phase (Fig. 7, *B* (*lanes 3–6*) and *C*), both of which have been shown to be inducible by p63 (29). These results were in agreement with the time lapse imaging results and suggest that IFN-α initiates its action during the S/G_2/M phase and that cell cycle arrest and apoptosis occur in the subsequent G_0/G_1 phase. We detected significant up-regulation of STAT1/2 expression and phosphorylation upon stimulation with IFN-α in both the G_0/G_1 and S/G_2/M phases (Fig. 8, *lanes 1–4*). In contrast, STAT3 was phosphorylated upon stimulation with IFN-α in both the G_0/G_1 and S/G_2/M phases, and total expression of STAT3 was not affected by IFN-α treatment. IFN-α-activated JAKs are also known to regulate the activation of Vav or other guanine nucleotide exchange factors, resulting in the regulation of p38 mitogen-activated protein kinase (MAPK) (5). Both the expression and phosphorylation of p38 were not changed by these treatments (Fig. 8, *lanes 7* and *8*), suggesting that these pathways may not be dependent on the cell cycle. To examine whether p63 can induce cell cycle arrest and apoptosis in HuH7 cells, we examined the mRNA expression of p21 and p53 up-regulated modulator of apoptosis (PUMA) in p63 (TAp63)-transfected HuH7 cells. Upon overexpression of TAp63, both p21 and PUMA were significantly up-regulated ~4.0- and 3.7-fold, respectively (Fig. 9), indicating the potency of TAp63 for inducing proapoptotic signaling in HuH7 cells.

To examine whether the apoptosis induced by IFN-α was dependent on p63, we performed knockdown experiments of p63. Expression of p63 was confirmed to be reduced in p63-knockdown cells (Fig. 10*A*), and p63-knockdown cells showed less activation of caspase-3 and -7 (Fig. 10*B*). This result clearly suggests that p63 was critically involved in apoptosis induced by the IFN-α/IFNAR2 signaling pathway.

DISCUSSION

IFN-α has been used in the clinic to treat HCC, indicative of its therapeutic potential. However, its actual modes of action are less clear, precluding further development of this line of novel therapies (30). Flow cytometric analysis is commonly used for studying the cell cycle, although we did not observe cell death events with this conventional methodology. This study is the first to use confocal time lapse cell cycle imaging analyses with Fucci to visualize the specific relationship between cell cycle and cell death. The results demonstrated that IFN-α exerts its action on IFNAR2-expressing tumor cells by first sensitizing cells in the S/G_2/M phases prior to inducing apoptosis in the G_1 phase. Combination therapy with IFN-α and 5-FU, commonly used clinically (30), can now be identified as an ideal regimen, because 5-FU is known to increase the S/G_2/M population (see Fig. 4), which makes the tumor cells more susceptible to IFN-α. The present evidence provides clinicians with the rationale for use of this combination therapy and enables them to further improve the regimen based on its mode of action.

However, this study raises new questions. Among them is how the action of IFN-α is dependent on the cell cycle. Biochemical analyses indicated that "cell cycle-independent" activation of STAT1/2 signaling with up-regulation of p63, a proapoptotic signaling molecule, was observed predominantly in the S/G_2/M phase. A promoter region of p63 reportedly contains putative binding motifs for E2F1, an E2F family transcription factor responsible for cell cycle regulation (31), although E2F1 may not bind to this motif by itself (32). Nevertheless, we can hypothesize that E2F1 or other cell cycle-dependent factors induce p63 expression if accompanied by STAT1 and -2 activation stimulated by IFN-α. On the other hand, it is also possible that the event of mitosis may be required for the induction of cell death by IFN-α. Further investigation is necessary to elucidate the whole picture of this intricate apoptotic signaling reg-

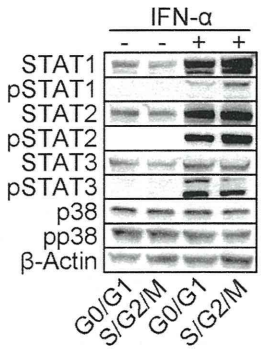

FIGURE 8. **Biochemical analyses of JAK/STAT and MAPK signaling.** The expression of several signaling molecules activated by IFN-α, including STAT1, phospho-STAT1 (*pSTAT1*), STAT2, phospho-STAT2 (*pSTAT2*), STAT3, phospho-STAT3 (*pSTAT3*), p38, phospho-p38 (*pp38*), and of β-actin (control) was analyzed by immunoblotting after culturing in the absence or presence of IFN-α (1,000 IU/ml) for 24 h. IFNAR2-expressing Fucci-introduced HuH7 cells were sorted by FACS for the G_0/G_1 (mKO single positive) or S/G_2/M (mAG single positive) samples.

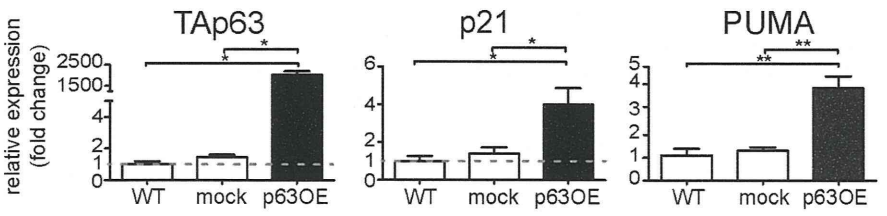

FIGURE 9. **Induction of proapoptotic factors, p21 and PUMA, by p63 in HuH7 cells.** Relative mRNA expression levels of TAp63, p21, and PUMA were detected by qPCR in wild-type HuH7 cells (*WT*) and in mock- or p63-overexpressing HuH7 cells (*p63OE*). Each *bar* represents the mean ± S.E. (*error bars*) of five individual experiments ($n = 5$ for each). *, $p < 0.05$; **, $p < 0.01$.

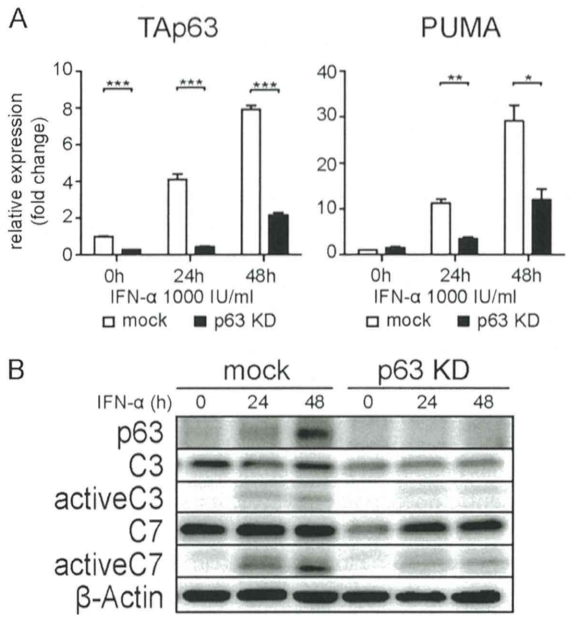

FIGURE 10. **Knockdown assay of p63 on IFNAR2-expressing HuH7 cells.** *A*, relative mRNA expression levels of TAp63 and PUMA in IFNAR2-expressing HuH7 cells after each time point of IFN-α (1,000 IU/ml) in p63 siRNA knockdown (*p63 KD*) and MISSION siRNA Universal Negative Control (*mock*). Each *bar* represents the mean ± S.E. (*error bars*) of triplicates. *B*, expression of apoptosis-related molecules in IFNAR2-expressing HuH7 cells measured by immunoblotting. p63-knockdown (*p63 KD*) or control cells (*mock*) were treated with IFN-α (1,000 IU/ml) for the indicated period of time. Protein levels of p63, caspase-3 (*C3*), active caspase-3, caspase-7 (*C7*), active caspase-7, and β-actin were measured by immunoblotting. *, $p < 0.05$; **, $p < 0.01$; ***, $p < 0.005$.

ulation associated with the cell cycle and controlled by therapeutic use of IFN-α.

Acknowledgments—We are grateful to Drs. A. Miyawaki and H. Miyoshi (RIKEN, Japan) for providing expression plasmids and advice and Drs. S. Seno and H. Matsuda (Osaka University) for image data analyses.

REFERENCES

1. Venook, A. P., Papandreou, C., Furuse, J., and de Guevara, L. L. (2010) The incidence and epidemiology of hepatocellular carcinoma: a global and regional perspective. *Oncologist* **15,** Suppl. 4, 5–13
2. Rehermann, B., and Nascimbeni, M. (2005) Immunology of hepatitis B virus and hepatitis C virus infection. *Nat. Rev. Immunol.* **5,** 215–229
3. Gutterman, J. U. (1994) Cytokine therapeutics: lessons from interferon α. *Proc. Natl. Acad. Sci. U.S.A.* **91,** 1198–1205
4. Pestka, S. (2007) The interferons: 50 years after their discovery, there is much more to learn. *J. Biol. Chem.* **282,** 20047–20051
5. Platanias, L. C. (2005) Mechanisms of type-I- and type-II-interferon-mediated signalling. *Nat. Rev. Immunol.* **5,** 375–386
6. Takaoka, A., Hayakawa, S., Yanai, H., Stoiber, D., Negishi, H., Kikuchi, H., Sasaki, S., Imai, K., Shibue, T., Honda, K., and Taniguchi, T. (2003) Integration of interferon-α/β signalling to p53 responses in tumour suppression and antiviral defence. *Nature* **424,** 516–523
7. Nagano, H., Miyamoto, A., Wada, H., Ota, H., Marubashi, S., Takeda, Y., Dono, K., Umeshita, K., Sakon, M., and Monden, M. (2007) Interferon-α and 5-fluorouracil combination therapy after palliative hepatic resection in patients with advanced hepatocellular carcinoma, portal venous tumor thrombus in the major trunk, and multiple nodules. *Cancer* **110,** 2493–2501
8. Ota, H., Nagano, H., Sakon, M., Eguchi, H., Kondo, M., Yamamoto, T., Nakamura, M., Damdinsuren, B., Wada, H., Marubashi, S., Miyamoto, A., Dono, K., Umeshita, K., Nakamori, S., Wakasa, K., and Monden, M. (2005) Treatment of hepatocellular carcinoma with major portal vein thrombosis by combined therapy with subcutaneous interferon-α and intra-arterial 5-fluorouracil: role of type 1 interferon receptor expression. *Br. J. Cancer* **93,** 557–564
9. Sangfelt, O., Erickson, S., and Grander, D. (2000) Mechanisms of interferon-induced cell cycle arrest. *Front. Biosci.* **5,** D479–D487
10. Kondo, M., Nagano, H., Wada, H., Damdinsuren, B., Yamamoto, H., Hiraoka, N., Eguchi, H., Miyamoto, A., Yamamoto, T., Ota, H., Nakamura, M., Marubashi, S., Dono, K., Umeshita, K., Nakamori, S., Sakon, M., and Monden, M. (2005) Combination of IFN-α and 5-fluorouracil induces apoptosis through IFN-α/β receptor in human hepatocellular carcinoma cells. *Clin. Cancer Res.* **11,** 1277–1286
11. Yano, H., Yanai, Y., Momosaki, S., Ogasawara, S., Akiba, J., Kojiro, S., Moriya, F., Fukahori, S., Kurimoto, M., and Kojiro, M. (2006) Growth inhibitory effects of interferon-α subtypes vary according to human liver cancer cell lines. *J. Gastroenterol. Hepatol.* **21,** 1720–1725
12. Sangfelt, O., Erickson, S., Castro, J., Heiden, T., Einhorn, S., and Grandér, D. (1997) Induction of apoptosis and inhibition of cell growth are independent responses to interferon-α in hematopoietic cell lines. *Cell Growth Differ.* **8,** 343–352
13. Murphy, D., Detjen, K. M., Welzel, M., Wiedenmann, B., and Rosewicz, S. (2001) Interferon-α delays S-phase progression in human hepatocellular carcinoma cells via inhibition of specific cyclin-dependent kinases. *Hepatology* **33,** 346–356
14. Sakaue-Sawano, A., Kurokawa, H., Morimura, T., Hanyu, A., Hama, H., Osawa, H., Kashiwagi, S., Fukami, K., Miyata, T., Miyoshi, H., Imamura, T., Ogawa, M., Masai, H., and Miyawaki, A. (2008) Visualizing spatiotemporal dynamics of multicellular cell-cycle progression. *Cell* **132,** 487–498
15. Morita, S., Kojima, T., and Kitamura, T. (2000) Plat-E: an efficient and stable system for transient packaging of retroviruses. *Gene Ther.* **7,** 1063–1066
16. Nishikawa, K., Nakashima, T., Hayashi, M., Fukunaga, T., Kato, S., Kodama, T., Takahashi, S., Calame, K., and Takayanagi, H. (2010) Blimp1-mediated repression of negative regulators is required for osteoclast differentiation. *Proc. Natl. Acad. Sci. U.S.A.* **107,** 3117–3122
17. Copeland, N. G., Gilbert, D. J., Schindler, C., Zhong, Z., Wen, Z., Darnell, J. E., Jr., Mui, A. L., Miyajima, A., Quelle, F. W., and Ihle, J. N. (1995) Distribution of the mammalian Stat gene family in mouse chromosomes. *Genomics* **29,** 225–228
18. Quelle, F. W., Thierfelder, W., Witthuhn, B. A., Tang, B., Cohen, S., and Ihle, J. N. (1995) Phosphorylation and activation of the DNA binding activity of purified Stat1 by the Janus protein-tyrosine kinases and the epidermal growth factor receptor. *J. Biol. Chem.* **270,** 20775–20780
19. Damdinsuren, B., Nagano, H., Wada, H., Noda, T., Natsag, J., Marubashi, S., Miyamoto, A., Takeda, Y., Umeshita, K., Doki, Y., Dono, K., and Monden, M. (2007) Interferon α receptors are important for antiproliferative effect of interferon-α against human hepatocellular carcinoma cells. *Hepatol. Res.* **37,** 77–83
20. Barchet, W., Cella, M., Odermatt, B., Asselin-Paturel, C., Colonna, M., and Kalinke, U. (2002) Virus-induced interferon α production by a dendritic cell subset in the absence of feedback signaling *in vivo*. *J. Exp. Med.* **195,** 507–516
21. Taylor, R. C., Cullen, S. P., and Martin, S. J. (2008) Apoptosis: controlled demolition at the cellular level. *Nat. Rev. Mol. Cell Biol.* **9,** 231–241
22. Shah, M. A., and Schwartz, G. K. (2001) Cell cycle-mediated drug resistance: an emerging concept in cancer therapy. *Clin. Cancer Res.* **7,** 2168–2181
23. Huberman, J. A. (1981) New views of the biochemistry of eucaryotic DNA replication revealed by aphidicolin, an unusual inhibitor of DNA polymerase α. *Cell* **23,** 647–648
24. Cagatay, T., and Ozturk, M. (2002) P53 mutation as a source of aberrant β-catenin accumulation in cancer cells. *Oncogene* **21,** 7971–7980
25. Yoshikawa, H., Nagashima, M., Khan, M. A., McMenamin, M. G., Hagiwara, K., and Harris, C. C. (1999) Mutational analysis of p73 and p53 in human cancer cell lines. *Oncogene* **18,** 3415–3421
26. Hagiwara, K., McMenamin, M. G., Miura, K., and Harris, C. C. (1999)

Mutational analysis of the p63/p73L/p51/p40/CUSP/KET gene in human cancer cell lines using intronic primers. *Cancer Res.* **59,** 4165–4169

27. Gressner, O., Schilling, T., Lorenz, K., Schulze Schleithoff, E., Koch, A., Schulze-Bergkamen, H., Lena, A. M., Candi, E., Terrinoni, A., Catani, M. V., Oren, M., Melino, G., Krammer, P. H., Stremmel, W., and Muller, M. (2005) TAp63α induces apoptosis by activating signaling via death receptors and mitochondria. *EMBO J.* **24,** 2458–2471
28. Deng, C., Zhang, P., Harper, J. W., Elledge, S. J., and Leder, P. (1995) Mice lacking p21CIP1/WAF1 undergo normal development, but are defective in G_1 checkpoint control. *Cell* **82,** 675–684
29. Dohn, M., Zhang, S., and Chen, X. (2001) p63α and ΔNp63α can induce cell cycle arrest and apoptosis and differentially regulate p53 target genes. *Oncogene* **20,** 3193–3205
30. Nagano, H., Wada, H., Kobayashi, S., Marubashi, S., Eguchi, H., Tanemura, M., Tomimaru, Y., Osuga, K., Umeshita, K., Doki, Y., and Mori, M. (2011) Long-term outcome of combined interferon-α and 5-fluorouracil treatment for advanced hepatocellular carcinoma with major portal vein thrombosis. *Oncology* **80,** 63–69
31. Waltermann, A., Kartasheva, N. N., and Dobbelstein, M. (2003) Differential regulation of p63 and p73 expression. *Oncogene* **22,** 5686–5693
32. Fogal, V., Hsieh, J. K., Royer, C., Zhong, S., and Lu, X. (2005) Cell cycle-dependent nuclear retention of p53 by E2F1 requires phosphorylation of p53 at Ser^{315}. *EMBO J.* **24,** 2768–2782

脂肪由来間葉系幹細胞を用いた細胞療法の膵島移植への応用
CD90high 脂肪由来間葉系幹細胞亜分画の有効性

川本弘一[*1)]，今野雅允[*2)]，石井秀始[*2)]，富丸慶人[*1)]，濱　直樹[*1)]，和田浩志[*1)]，小林省吾[*1)]，江口英利[*1)]，種村匡弘[*3)]，伊藤壽記[*4)]，森　正樹[*1)]，土岐祐一郎[*1)]，永野浩昭[*1)]

REVIEW ARTICLE

Possible application of adipose-derived mesenchymal stem cells to islet transplantation—potential of CD90 high-expression cells

〔Abstract〕 Mesenchymal stem cells (MSCs), including adipose tissue-derived mesenchymal stem cells (ADSC), are multipotent and can differentiate into various cell types possessing unique immunomodulatory features. Several clinical trials have demonstrated the safety and possible efficacy of MSCs in organ transplantation. Thus, stem cell therapy is promising for tolerance induction. In this study, we assessed the reprogramming capacity of murine ADSCs and found that CD90 (Thy-1), originally discovered as a thymocyte antigen, could be a useful marker for cell therapy. Murine ADSCs were isolated from B6 mice, sorted by selection of CD90Hi or CD90Lo, and then transduced with four standard factors (Oct4, Sox2, Klf4, and c-Myc). Among unsorted, CD90Hi-, and CD90Lo- murine ADSCs, reprogrammed CD90Hi ADSCs showed increased numbers of alkaline phosphatase-positive colonies compared with reprogrammed CD90Lo ADSCs. The relative reprogramming efficiencies of unsorted, CD90Hi-sorted, and CD90Lo-sorted ADSCs were 100%, 116.5%, and 74.7%, respectively. CD90Hi cells were more responsive to reprogramming. CD90Hi ADSCs had greater reprogramming capacity than CD90Lo ADSCs, suggesting that ADSCs have heterogeneous subpopulations. Thus, CD90Hi selection presents an effective strategy to isolate a highly suppressive subpopulation for stem cell-based tolerance induction therapy.

key words: CD90, ADSC, reprogramming
(CD90, 脂肪由来間葉系幹細胞, リプログラミング)

Koichi Kawamoto[*1)], *Masamitsu Konno*[*2)], *Hideshi Ishii*[*2)], *Yoshito Tomimaru*[*1)], *Naoki Hama*[*1)], *Hiroshi Wada*[*1)], *Shogo Kobayashi*[*1)], *Hidetoshi Eguchi*[*1)], *Masahiro Tanemura*[*3)], *Toshinori Ito*[*4)], *Yuichiro Doki*[*1)], *Masaki Mori*[*1)], *Hiroaki Nagano*[*1)]

1 型糖尿病に対するβ細胞代替療法

1 型糖尿病の本体は，自己免疫を原因とするインスリン産生細胞(β細胞)の破壊であり，最終的には自己反応性 T 細胞によりβ細胞は全滅し，内服治療は無効である．したがって，1 型糖尿病に対する標準療法はインスリン強化療法となる．インスリン強化療法は，糖尿病性合併症の進行を抑制可能であるが，時として低血糖発作が頻発し，致命的になることもある．このことは，1 型糖尿病に対するインスリン治療の限界を示している．

インスリン強化療法に対して，24 時間連続的に血糖値をモニターしつつ，それに対して必要充分なインスリンを分泌させる機能を有する細胞を患者に移植することで，完璧な血糖コントロールを回復させることを目的とした治療法がβ細胞代

[*1)] Department of Surgery, Graduate School of Medicine, Osaka University; 大阪大学大学院医学系研究科消化器外科
[*2)] Department of Frontier Science for Cancer and Chemotherapy, Graduate School of Medicine, Osaka University; 大阪大学大学院医学系研究科消化器癌先進化学療法開発学
[*3)] Department of Surgery and Institute for Clinical Research, National Hospital Organization Kure Medical Center and Chugoku Cancer Center; 独立行政法人国立病院機構呉医療センター中国がんセンター外科
[*4)] Department of Complementary and Alternative Medicine, Graduate School of Medicine, Osaka University; 大阪大学大学院医学系研究科生体機能補完医学